Radiative muon capture in nuclei

M. Döbeli, M. Doser, L. van Elmbt,* M. W. Schaad,† and P. Truöl
Physik Institut der Universität Zürich, 8001 Zürich, Switzerland

A. Bay‡ and J. P. Perroud
Institut de Physique Nucléaire, Université de Lausanne, 1015 Lausanne, Switzerland

J. Imazato§ and T. Ishikawa
Department of Physics and Meson Science Laboratory, Faculty of Science, University of Tokyo, Tokyo 113, Japan
(Received 26 October 1987)

The energy spectra of photons following negative muon absorption in ^{12}C, ^{16}O, ^{27}Al, ^{40}Ca, ^{nat}Fe, ^{165}Ho, and ^{209}Bi have been measured with two NaI spectrometers. The branching ratios for the emission of high energy photons give information on the induced pseudoscalar coupling constant g_P in nuclear matter. The data for light nuclei are in agreement with the theoretical calculations using the nucleonic value of $g_P \approx 7 g_A$ predicted by the partially conserved axial vector current hypothesis, while significantly lower values of g_P are required to fit the data of the heavier elements with presently existing theoretical predictions. Disregarding the remaining theoretical uncertainties, these results can be interpreted as a further indication of the renormalization of the nucleonic form factors inside the nucleus.

I. INTRODUCTION

Investigations of the rare radiative muon capture process continue to be justified due to their connections with the induced pseudoscalar branch of the semileptonic weak interaction. Essentially only ordinary muon capture delivers also some information on the induced pseudoscalar coupling constant g_P for which the partially conserved axial vector current hypothesis (PCAC) predicts a value of $g_P \approx 7 g_A$ (e.g., Ref. 1) at the momentum transfer corresponding to ordinary muon capture on the proton ($q^2 = -0.88 m_\mu^2$). The average of the latest measurements of the orthomolecular capture rate for muonic hydrogen[2] yielded a value for g_P/g_A of 7.0 ± 1.5. The only other data points are $g_P/g_A = 9.0 \pm 1.7$ [from the $^{12}C(\mu^-,\nu_\mu)^{12}B$(g.s.) capture rate and the recoil polarization[3]] and $g_P/g_A \approx 12.5$ [from the $^{16}O(\mu^-,\nu_\mu)^{16}N(0^-)$ capture rate and the $^{16}N(0^-)$ β decay[4]]. In contrast to ordinary muon capture, the momentum transfer can be varied from $q^2 = -0.9 m_\mu^2$ to $q^2 = 0.9 m_\mu^2$ in the radiative capture process which enhances the pseudoscalar coupling by up to a factor of ~ 3.5 at the maximum photon energy by virtue of the pion pole. As a consequence the photon yield, the photon polarization, as well as the photon muon-spin angular correlation in radiative muon capture, are particularly sensitive to the value of g_P.

Unfortunately the low capture probability in hydrogen ($\sim 10^{-3}$) together with the low expected photon yield ($\sim 10^{-5}$ per captured muon) prohibited the direct investigation of the elementary radiative capture process $p(\mu^-,\nu_\mu\gamma)n$ until now. Experiments become easier if the muon is captured on heavier nuclei for which the capture probability is enhanced by up to 3 orders of magnitude.[5] However, the advantage of higher capture rates is partially balanced by the theoretical difficulties arising through the modification of the elementary process by the nuclear medium (non-nucleonic degrees of freedom) and the effort needed to account correctly for the distribution of nuclear final states which have not been experimentally resolved.

Most theoretical, as well as experimental, work concentrated on the doubly closed shell nucleus ^{40}Ca. The first reliable measurement for this nucleus in 1977 (Ref. 6) with a NaI spectrometer obtained an integrated yield of $B_\gamma = (2.11 \pm 0.14) \times 10^{-5}$ for photons with energies above 57 MeV. This value was later confirmed with a high resolution pair spectrometer.[7] The later data agreed with theoretical calculations[8,9] with $g_P/g_A = (4.0 \pm 1.5)$, indicating some quenching of the induced pseudoscalar coupling in nuclei. Such a renormalization, if indeed confirmed by further data, would, of course, provide additional input for the ongoing discussion of the possible modification of nucleonic properties in nuclear media, apparent, e.g., in the EMC effect, in the suppression of the longitudinal response in inelastic electron scattering or in the missing Gamow-Teller strength in nucleon charge exchange reactions.[10] The induced pseudoscalar coupling is particularly suited to study the distortion of the pion field inside the nucleus,[11-13] since it is dominated by one pion exchange as mentioned above.

These considerations initiated the measurements of the radiative muon capture yield for a series of nuclei spread over the periodic system, which we report on in the following. It was hoped, that the extension of the yield measurements to nuclei other than ^{40}Ca will eliminate or expose the dependence of the calculations on the details of the nuclear response.

A complete review of the current theoretical and experimental situation in radiative muon capture is given in Ref. 14, some aspects of the theoretical discussion important to our experiment, however are repeated for clarification in the following.

 ©1988 The American Physical Society

II. THEORETICAL MODELS

In most of the presently existing calculations of radiative muon capture (RMC) the *impulse approximation* is applied, i.e., the relevant amplitude for a free proton is summed over all nucleons within the nucleus. The nonrelativistic reduction of this amplitude presents no extraordinary problems. Several theoretical approaches (e.g., Refs. 15–17) lead to very similar results differing only by higher order terms which are insignificant compared to the presently available experimental precision.

In the impulse approximation interactions involving more than one nucleon (e.g., scattering of the exchange pion) are neglected. To account for meson exchange corrections (MEC) most often renormalized quasiparticle form factors for the nucleon inside the nucleus are used.[13,18–20] In the test case of the medium heavy ^{40}Ca nucleus Akhmedov *et al.*[20] found a reduction of the branching ratio of the radiative capture of 10–12 % caused by the MEC connected with the weak interaction vertex while an earlier work by Ohta[19] obtained a 30–40 % reduction. The corrections induced by the MEC at the electromagnetic vertex seem more important. Gmitro *et al.*[9] developed a modified version of the impulse approximation (MIA) relying on constraints imposed by the electromagnetic continuity equation, which accounts for a large part of these MEC and leads to a reduction of the rate by almost a factor of 2 for ^{40}Ca. It is with respect to this theory that the further quenching of g_P is required by the data, in contrast to the estimation of Akhmedov *et al.*[20]

Since measurements of the radiative capture to exclusive nuclear final states do not exist, one has to sum the RMC amplitudes over all possible final states. In the calculations referred to above[9,20] (1p1h)-shell model states with a doubly closed ^{40}Ca ground state were considered. Earlier treatments resorted to the *closure approximation,* where one assumes that all existing nuclear final states can be reached by the radiative capture and the nuclear excitation energy is substituted by a common mean implying one single maximum photon energy k_{max}. This method consistently overestimates the experimental rate for ^{40}Ca and its deficiencies were exposed both in experimental[7] as well as in theoretical work.[8] A better technique based on a phenomenological nuclear response function first applied to normal muon capture by Foldy and Walecka[21] was used in RMC calculations by Christillin[8] for ^{40}Ca (we shall refer to this model by "Chr81"). Here the nuclear response is divided into a giant dipole and a quadrupole resonance part with width and strength adjusted to the photonuclear giant dipole resonance and the total muon capture rate. Kinematically forbidden photon energies appearing in the simple closure approximation are avoided by transforming the summation over the final states into an integration over the accessible excitation energies. A refined version of this model was applied to the ^{16}O nucleus by Christillin and Gmitro[22] ("CG85") including the low lying states $0^-,1^-,2^-,3^-$ in ^{16}N. Shell model (MIA) (Ref. 9) and phenomenological response[8,22] lead to consistent descriptions for ^{16}O and ^{40}Ca.

In the absence of similar, highly developed theoretical calculations for the remaining nuclei (^{27}Al, ^{nat}Fe, ^{165}Ho, ^{209}Bi) investigated in this experiment, we refer to the results of a comparatively simple Fermi-gas calculation by Christillin *et al.*[23] ("CRS80") to interpret our data in this case. In the actual data analysis we make use of the fact, that the shape of the photon spectrum is nearly independent of the nuclear model. The nuclear model determines primarily the rate. In fact the simple polynomial form

$$\frac{d\Lambda}{dk}(x)\sim(1-2x+2x^2)x(1-x^2),\quad x=\frac{k}{k_{max}}$$

which results from the closure approximation[15] approximates the full calculation very well, provided that k_{max} is properly chosen. This is shown in Fig. 1 for ^{16}O and a heavier nucleus. The Fermi-gas model estimates indicate that the sensitivity of the rate to the value of g_P persists to heavier nuclei. Since the density of accessible final

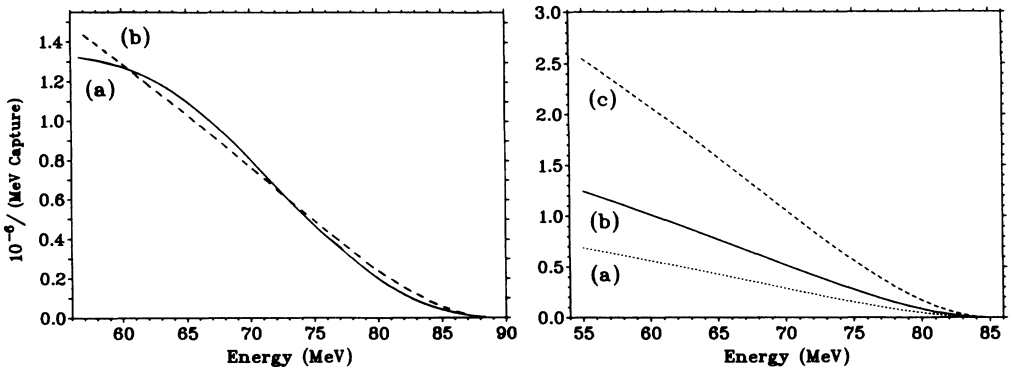

FIG. 1. Calculated μ-capture photon yield as a function of the photon energy. Left: CG85 (Ref. 22) (see text) for ^{16}O and $g_P=7g_A$ (a) compared to the simple polynomial (b) with the same integral yield. Right: Polynomial form with integral yield calculated by CRS80 (Ref. 23) (see Fig. 14) for ^{nat}Fe and (a) $g_P=0$, (b) $g_P=7g_A$, (c) $g_P=14g_A$.

states is particularly large in this case, it is hoped that the global treatment suffices to characterize the nuclear response and that rate measurements provide a meaningful measure of g_P in a nuclear environment.

III. EXPERIMENTAL ASPECTS

A. Experimental set up

The requirements for radiative muon capture experiments are largely dictated by the low photon yield, the intense background of neutrons and bremsstrahlung from muon decay electrons. The experiment was carried out in the $\mu E1$ zone of the muon facility of the Swiss Institute for Nuclear Research at Villigen (SIN) which offers a high intensity μ^- beam at a momentum of 125 MeV/c with a range width of 4.5 g/cm^2 full width at half maximum (FWHM). The incident muon rate can be varied by means of an intensity slit system in the beamline from 350 kHz up to $\sim$30 Mhz at a primary proton current of 150 μA The muons arrive in 3.5 nsec wide bunches with a repetition frequency of 50 Mhz. The electron contamination of the beam is lower than 1% and we measured a pion contamination of the order of 5×10^{-4}.

As Fig. 2 illustrates, the beam entered the experimental area via a first counter hodoscope (μ_1) consisting of six 5 mm thick plastic scintillator strips with individual photomultiplier (PM) tubes in order to reduce the counting rates. Through a second defining counter μ_2 ($100\times100\times5$ mm^3) the beam passed into a 10 cm long polyethylene degrader and then partially stopped in the target in a spot of $\sim$70 mm diameter. The ^{12}C, ^{27}Al, ^{40}Ca, ^{nat}Fe, and ^{209}Bi targets were tricline plates of 70×85 mm^2 placed under 45° to the beam with a surface density of $\sim$5 g/cm^2. The ^{165}Ho target was a thin plate of only 1.9 g/cm^2 surface density. The ^{16}O target was actually a thin-walled polyethylene container ($65\times65\times50$ mm^3) filled with water. The target was surrounded by a closed cubic scintillator box of 1 mm wall thickness. The front part of this target box defined the entrance of a particle (μ_3) while the rear five faces of the cube (μ_4) vetoed the particles passing through the target. After determination of the stop rates per μ_1 this target box was replaced by a synthetic foam support (0.002 g/cm^3) to avoid background events. The degrader was adjusted then to account for the missing stopping power of μ_3.

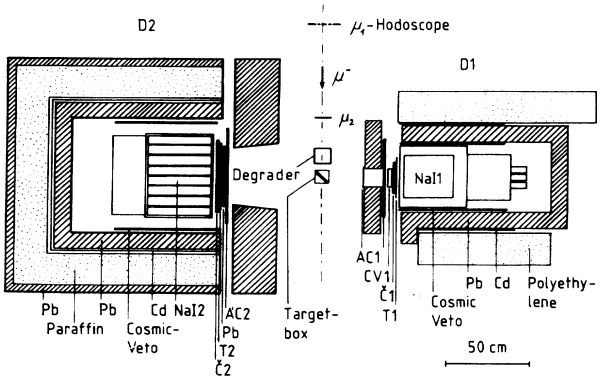

FIG. 2. Experimental set up.

Two detector systems were placed perpendicularly to the beam axis. The first (D1) consisted of a single cylindrical NaI crystal (27 cm diameter, 33 cm length) (NaI1) with seven PM tubes. It was surrounded by four $55\times60\times1$ cm^3 cosmic veto counters and shielded by a 10 cm lead, 2 mm cadmium, and 20 cm polyethylene housing. It was separated from the target by an 11×11 cm^2 lead collimator (10 cm thick) with a scintillation counter (AC1) at each end to veto charged particles.

Behind the collimator a photon converter telescope was installed in order to distinguish photons from neutrons: A small cylindrical NAI crystal (12 cm ϕ, 2 cm length) (CV) converted about a third of the high energy photons into electron-positron pairs. A 1 cm plastic Čerenkov counter (Č1) then discriminated these electrons from possible recoil protons due to neutron scattering. In order to confirm the CV-Č1 coincidence a 2 mm scintillation counter (T1) completed the telescope and provided a sharp timing signal. A photon trigger was thus released by an $\overline{AC1}\times CV\times\check{C}1\times T\times NaI1$ coincidence. The pulses of all these counters (except the veto counters) were fed to charge sensitive analog-to-digital converter (ADC's). In addition, the time between the passage of a beam particle through μ_1 and the event was recorded together with the time elapsed since the last accelerator synchronization pulse. Event data were transferred to magnetic tape via a CAMAC system and a PDP 11/40 processor.

The opposite detector (D2) consisted of a 8×8 matrix of $6.35\times6.35\times40.6$ cm^3 NaI bars with individual PM tubes (NaI2, NaI wall). This detector and the associated electronics is described in detail elsewhere.[24] The shielding was very similar to the one of D1, but was reinforced by an additional layer of 5 cm lead. The photon telescope of D2 did not include an active converter. The place of the small NaI crystal was taken here by a 4 mm lead sheet. Consequently, a photon signal was given by $\overline{AC2}\times\check{C}2\times T2\times NaI2$. Each NaI module had its own ADC and TDC. The pulse height of Č2 and T2 were recorded, too. The sum of the energy deposits in all hit bars was corrected by a Monte Carlo calculation for the energy loss in the lead converter. For the ^{12}C target we used a 6 mm lead converter for D2. Consequently, the detector acceptance and resolution differs. Since the final number of events for ^{12}C is quite small and the result rather marginal, we have omitted a detailed discussion of this data set in the following (see, however, Ref. 25).

B. Calibration and detector features

The determination of the muon stop rates in the target per μ_1, the only beam counter able to support the maximum particle rates, presented some specific problems. At an incident muon intensity of 30 MHz the counting rates in the six μ_1 hodoscope strips had to be corrected for counting losses. We studied this effect by comparing the μ_1 rates with those of a counter monitoring the primary proton current at the production target. The μ_1 counting rate in function of the beam intensity was very well fitted by a first order deadtime correction, amount-

ing to 23% at the maximum intensity of 30 MHz. We determined the fraction of muons stopping per μ_1 at reduced muon intensity using the scintillator box described above. To reduce the intensity apertures were introduced in the muon channel upstream of the last focusing elements. Since such a procedure may affect the phase space density of the beam, we normalized the stop rates without aperature to those with aperture by using the number of observed electrons from muon decay in the target. Electron events in our detectors could easily be selected by switching the veto counters (AC1, AC2) from anticoincidence to coincidence in the trigger. We reached a typical precision for the number of muon stops relevant for a measured spectrum of ±7%. For Al we had to assign a larger upper error (+19%) because we could not rule out that the data were erroneously taken with a thinner (18% less stopping power) target than used during the range measurement.

The energy calibrations, the resolution functions, the absolute acceptance and the neutron rejection of our photon spectrometers was derived from radiative pion capture (RPC) in hydrogen obtained by subtracting carbon data from polyethylene data (see Fig. 3). For this purpose the muon channel had to be tuned to the primary pion momentum. The pulsed structure of the beam allowed to discriminate pion stops in the target against the considerable electron and muon contamination by time of flight selection relative to the accelerator radiofrequency signal.

The energy calibration of D1 was performed as follows: For the large cylindrical crystal the photon line at 129.4 MeV from the reaction $\pi^- p \rightarrow n\gamma$ and the end points of the continuous spectrum from the charge exchange process $\pi^- p \rightarrow n\pi^0; \pi^0 \rightarrow 2\gamma$ at 55 and 83 MeV provide three reference points. For this, events with an additional signal in any other converter telescope counter were excluded. At 130 MeV an energy resolution of $\Delta E/E(\text{FWHM})=9\%$ was found. We monitored this calibration with frequent measurements of the energy spectrum of cosmic muons traversing the crystal which provided a relatively sharp peak at about 100 MeV. During eight days of operation this peak shifted by 2 MeV which was accounted for. The small NaI converter was calibrated with the energy loss signal of decay electrons passing through the counter corresponding to 11 MeV. Daily repetitions of electron runs proved this counter to be stable.

The total energy of a photon event in D1 was given by the sum of the deposited energies in the two NaI crystals plus a correction for the mean energy loss in the other converter telescope counters and the aluminum housings of the crystals. Since the mean number of electrons and positrons in the shower and, hence, the energy loss, increases with the incident photon energy, we made the following ansatz for the true photon energy in D1:

$$E_\gamma = E'_\gamma + \omega_1 + \epsilon_1 E'_\gamma \ ,$$

where E'_γ is the sum of the measured energies in the converter and the big NaI. We determined ω_1 to 5.8 ± 0.8 MeV and ϵ_1 to $(5.1\pm0.4)\times10^{-2}$ with a fit to the measured RPC spectrum on hydrogen which is displayed in Fig. 3. The theoretical spectrum was folded with a phenomenological resolution function that, for an incident photon energy E_0 is of the form

$$R_1(E_0,E)=A\exp\left[-\frac{1}{2\sigma^2}(E-E_0)^2\right] \quad \text{for } E>E_t$$

$$R_1(E_0,E)=A\exp\left[-\frac{1}{2\sigma^2}(E-E_0)^2\right] \times\exp\left[\frac{1}{2\sigma^2}(E-E_t)^2\right] \quad \text{for } E<E_t \ ,$$

which is essentially a Gaussian with a low energy tail. $E_t=0.76\sigma$, A is a normalization constant and the width of the resolution function is assumed to be of the form

$$\frac{\Delta E}{E_0}(\text{FWHM})=2.35\times\frac{\sigma}{E_0}=\left[\alpha_1+\frac{\beta_1}{E_0}\right]^{1/2} .$$

The fit yielded a value $\Delta E/E_0=11\%$ at 130 MeV with $\alpha_1=-0.011$ and $\beta_1=3.0$ MeV. The detector resolution as a function of the energy is displayed in Fig. 4.

The time and energy calibration procedure of the NaI

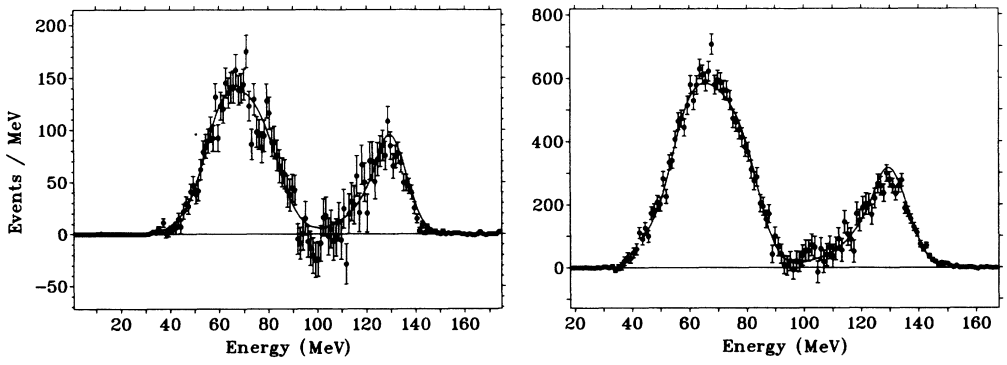

FIG. 3. Radiative pion capture spectra from hydrogen (left: D1, right: D2). Result of a CH_2-C subtraction. The solid lines are fits of the theoretical spectrum folded with a phenomenological resolution function for D1 and a Monte Carlo calculation for D2.

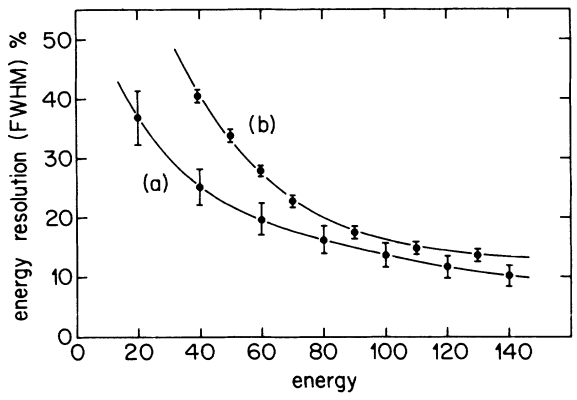

FIG. 4. Detector resolution in function of the photon energy. A result of a fit to the hydrogen RPC spectrum for (a) D1 and from a Monte Carlo simulation for (b) D2.

wall (D2) is slightly more complex, as detailed in Ref. 24. In order to optimize the event timing with respect to the accelerator synchronization signal and to the μ_1 counter we first adjusted the TDC histograms of the individual bars to a common time scale by means of the RCP photon time of flight peaks. We then calibrated the energy of each of the 64 NaI modules with three lines from γ sources (^{137}Cs, ^{88}Y) and with the peak produced by cosmic muons passing through a whole row of bars (the position of this peak was known from an earlier measurement[24]). Events in the NaI wall were then processed as follows: First all modules containing less than 2 MeV were discarded. Among the remaining bars the one with the maximum energy deposit was searched. The corresponding TDC determined the event timing. In order to suppress noise and event pile up only those bars which fired within ± 10 nsec with respect to the bar containing the maximum energy were kept for the calculation of the total energy and the centroid of the photon shower. Events with a centroid lying nearer than 6.35 cm to the surface of the crystal array were excluded to avoid shower escape.

Since the unknown energy loss of the photon shower in the lead converter and the telescope counters was appreciable and strongly dependent on the position of the photon conversion vertex, we simulated the detector response with an electron photon shower Monte Carlo program (EGS) developed at Stanford Linear Accelerator Center (SLAC) (Ref. 26). We generated sets of 30 000 events with photon energies E_γ of 10, 20, . . ., 140 MeV entering the spectrometer via the lead converter. The generated response was fitted best by a resolution function of the following form:

$$R_2(E_\gamma,E)=A\exp\left[-\frac{1}{2\sigma_1^2}(E-E_0)^2\right] \quad \text{for } E>E_t\ ,$$

$$R_2(E_\gamma,E)=B\exp\left[-\frac{1}{2\sigma_2^2}(E_t-E)\right] \quad \text{for } E<E_t\ ,$$

with

$$E_t=E_0-\frac{\sigma_1^2}{2\sigma_2}$$

and

$$B=A\exp\left[-\frac{(E_t-E_0)^2}{\sigma_1^2}\right],$$

where A, E_0, σ_1, and σ_2 are free parameters. The fitted parameters are displayed in function of the photon energy in Fig. 5. The solid lines correspond to the following parametrization of the resolution function $R_2(E_\gamma,E)$:

$$E_\gamma-E_0=\omega_2+\epsilon_2 E_\gamma,\quad \omega_2=17.6\text{ MeV},\quad \epsilon_2=0.051\ ,$$

$$\sigma_1=\alpha_2+\beta_2 E_\gamma,\quad \alpha_2=3.7\text{ MeV},\quad \beta_2=0.020\ ,$$

$$\sigma_2=\phi+\delta E_\gamma,\quad \phi=6.1\text{ MeV},\quad \delta=0.022\ .$$

In addition, the simulation provided the energy dependence of the detector acceptance. We established the final energy calibration by fitting the measured hydrogen RPC spectrum with the above parametrization of the resolution function leaving ω_2 as a free parameter. In order to be sure that the calibration was as precise as possible in the RMC energy region we included only the π^0 decay spectrum in the fit. This fixed ω_2 to 18.1 ± 0.7 MeV (Fig. 3) in quite good agreement with the simulated value.

The absolute acceptance a_1 of the detector D1 was determined with a measurement of the RPC yield from a carbon target comparing it to the average of all published values of $(1.77\pm0.06)\times10^{-2}$ (Ref. 27) with the result $a_1=(1.18\pm0.09)\times10^{-3}$ at 130 MeV. This value needs to be corrected for the energy dependence of the photon conversion probability in NaI,[28] the photon self-absorption in the target (2%) and the higher low energy threshold of NaI (22 MeV) used for μ-capture runs to suppress bremsstrahlung backgrounds. The resulting acceptance is displayed in Fig. 6.

The acceptance a_2 of D2 was normalized with the measured photon yield from pion capture in hydrogen resulting from the CH_2-C subtraction. In this way we avoided the correction for the loss of carbon events in the low energy region due to the high trigger threshold. Folding the theoretical spectrum with the parametrized resolu-

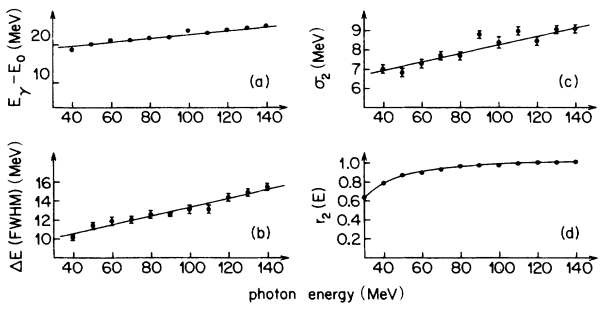

FIG. 5. Parametrization of the resolution function of D2 in function of the photon energy determined by a Monte Carlo simulation. (a) Mean energy loss in the converter telescope, (b) resolution (FWHM), (c) length of the low energy tail, and (d) detector acceptance normalized to 1.0 at 130 MeV.

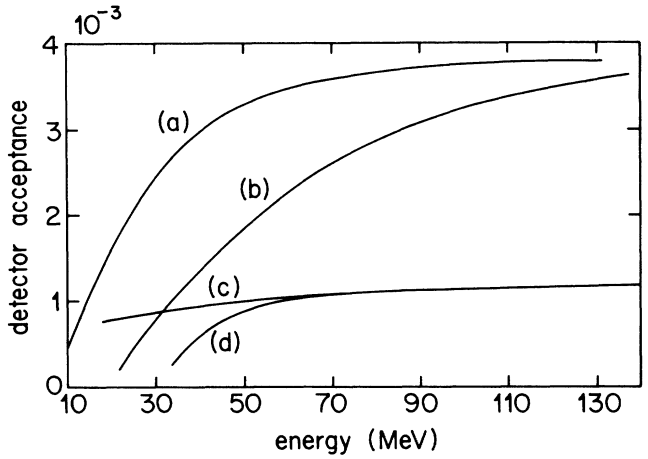

FIG. 6. Detector acceptances in function of the photon energy. (a) For D2, (b) for D2 with at least three bars hit, (c) for D1, and (d) for D1 with a low energy threshold of 22 MeV in NaI1.

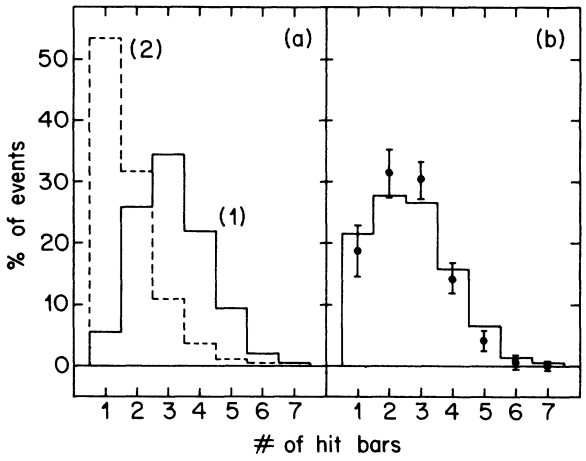

FIG. 7. (a) Hit bars distribution for 60–70 MeV photons (1) and neutrons (2). (b) Hit bars for μ-capture events of the same energy from ^{165}Ho. The solid line is a fit with a mixture of photons and neutrons.

tion function gave $a_2=(3.80\pm0.33)\times10^{-3}$ at 130 MeV using a value of $1.26\pm0.06\%$ for the probability of pion capture on a proton in CH_2 (Ref. 29) and 0.605 ± 0.003 for the branching ratio for the charge exchange process.[30]

A severe problem in RMC experiments can be caused by the high neutron background resulting from ordinary muon capture. For ^{40}Ca the neutron production rate in an energy interval between 55 and 90 MeV is about 100 times higher than the photon yield.[31] Therefore, the neutron sensitivity of our detectors was investigated also with the pion beam. Neutral products of the prompt π-capture process in the carbon target could be well identified by their time of flight (TOF) difference to the detectors (e.g., 75 MeV neutrons had a TOF difference to photons of $\sim$2.5 nsec for D1 and $\sim$3.5 for D2). By switching the conversion telescopes off we determined the number of neutron events in the energy region between 60 and 90 MeV among nonconverted events. Using the neutron detection efficiency of NaI ($\sim6.3\times10^{-4}$ cm^{-1}) (Ref. 32) we then estimated the approximate number of neutrons emitted into the detectors' solid angle. The comparison to the number of events with a neutron TOF, seen with the conversion telescopes on, yielded directly the neutron detection efficiency of our detectors, which was $<4\times10^{-5}$ for D1 (we actually did not see any clearly identified neutron events in D1) and 4×10^{-4} for D2. The fairly high neutron sensitivity of D2 was caused by neutrons producing recoil protons in the trigger counter T2 which were able to fire the Čerenkov counter by knock-on electrons. A calculation performed with a theoretical model for knock-on electron production[33] reproduced the right order of magnitude for the observed probability and the correct energy dependence of the process (the neutron sensitivity strongly decreased with energy).

The modular structure of the NaI wall, however, offered the possibility to suppress and determine the neutron background in photon spectra quantitatively. As Fig. 7 illustrates, the distribution of the number of NaI bars that participate in an event clearly discriminates photon showers from the spatially well confined recoil proton events.

We consequently used sets of our muon capture data including only events that involved at least three bars, a condition which reduced the neutron sensitivity by 85%. The altered detector acceptance for the reduced data sets can easily be investigated by reanalyzing the neutron free RPC spectra (cf. Fig. 6).

IV. DATA REDUCTION

A. Background analysis

In order to make the data analysis procedure clear the composition of the measured photon spectra [Fig. 8(a)] is shortly described in the following:

An appreciable part of the stopped muons in the target material decay in the atomic orbit (Table VI). The lower part of the energy spectrum is therefore completely dominated by the electron bremsstrahlung from normal muon decay $\mu^-\rightarrow e^-\bar{\nu}_e\nu_\mu$ and by photons from the radiative muon decay $\mu^-\rightarrow e^-\bar{\nu}_e\nu_\mu\gamma$. The spectral shape of the two contributions is rather similar, but the radiative decay is negligible compared to the outer bremsstrahlung for a mean path of the decay electron of 0.06 (^{12}C) to 0.29 (^{209}Bi) radiation lengths through the target.[7] For a free muon the bremsstrahlung spectrum cuts off at half the muon mass, but for a bound muon it extends to slightly higher energies[34] (Fig. 9).

Between 60 and 100 MeV the major part of the spectrum consists of radiative muon capture photons. Because of the comparatively high RPC branching ratios of the order of $\sim2\times10^{-2}$ (Ref. 27) a pion contamination of 5×10^{-4} in the muon beam is sufficient to produce a photon background of the same order of magnitude as the RMC signal which is expected to be in the range of 10^{-5} per captured muon. The neutron events in D2 fall into this same energy region.

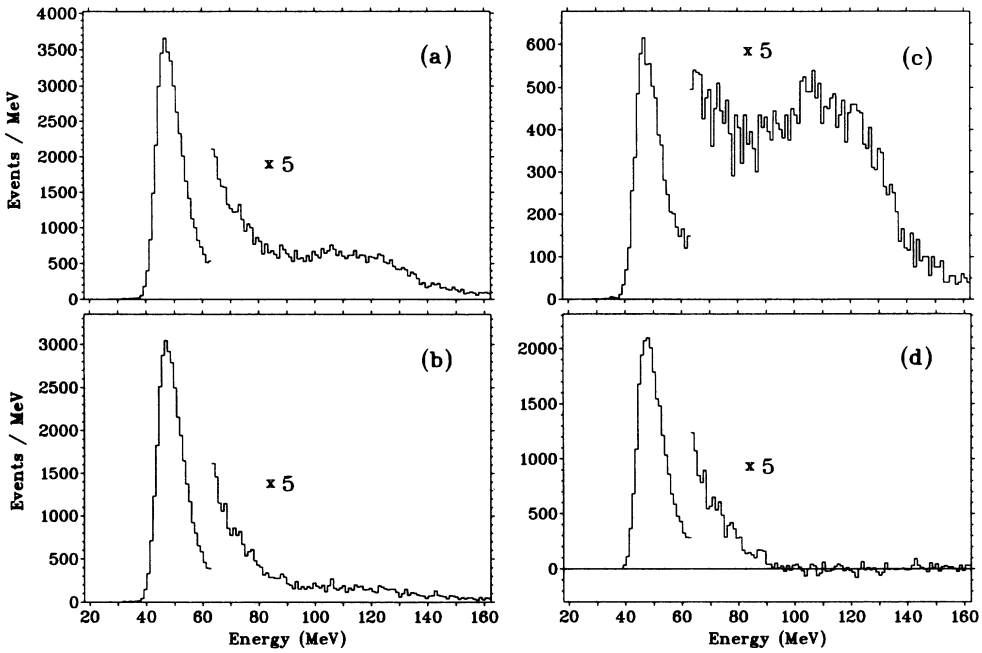

FIG. 8. Measured photon energy spectra from muons stopped in ^{nat}Fe (a) all events, (b) nonprompt events, (c) prompt events, and (d) prompt events subtracted.

Above ~100 MeV RMC photons are energetically forbidden but RPC photons are still present up to nearly the pion mass.

Cosmic muons passing through the light guides of Č2 and T2 into the NaI wall were able to trigger the photon conversion telescope by Čerenkov light. Measurements with the accelerator off showed that most of these events had energies higher than 200 MeV.

1. *Bremsstrahlung*

We generated EGS simulated bremsstrahlung spectra starting from decay electron spectra of bound muons as calculated in Ref. 34 and using the measured muon stop density in the targets (Fig. 9, left). A first χ^2 fit of the predicted RMC spectra with an admixture of these bremsstrahlung spectra to the low energy part of our data determined the energy limit above which the contribution of bremsstrahlung is negligible (Fig. 9, right). Because of the relatively bad resolution of our detectors (e.g., in contrast to the pair spectrometer measurements[7]) these limits were rather high (~65 MeV) compared to the approximate limit given by $m_\mu/2$.

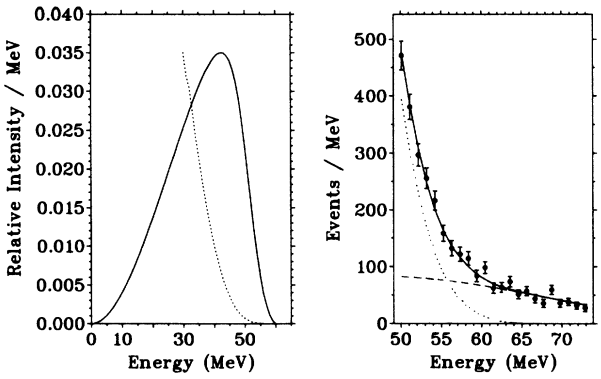

FIG. 9. Decay electron spectrum calculated according to Ref. 34 (solid curve, left) and the resulting EGS generated bremsstrahlung energy spectrum for the ^{nat}Fe target (dotted curve). In the right figure the calculation is compared to the data [dotted: bremsstrahlung, dashed: RMC following (Ref. 23) (CRS80), solid line: sum].

2. *Subtraction of pion capture events*

RPC events can be identified by their prompt time structure. Figure 10 shows the time distribution of photon events in respect to a beam particle arrival through the first beam counter. Selecting events within a window of about 10 nsec around the clearly visible "prompt" peak in the time spectrum enhances the high energy part of the photon spectrum as expected [Fig. 8(c)]. On the other hand, the selection of "nonprompt" events outside this window suppresses the high energy events, though not completely because of the limited efficiency of the beam counter. Yet the remaining pion capture events can be removed by subtraction of the prompt photon spectrum with a subtraction factor S_{pr} which is given by the ratio of nonprompt to prompt events in the energy region between 100 and 140 MeV. Hence, spectra without pion contribution are obtained as

$$\frac{dN'_\mu}{dE} = \frac{dN^{\text{nonprompt}}}{dE} - S_{pr}\frac{dN^{\text{prompt}}}{dE} .$$

Quantities related with the pion subtraction for the seven targets and for empty target measurements are list-

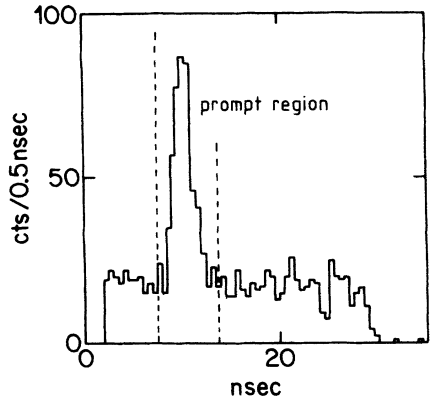

FIG. 10. Arrival time spectrum of photon events from ^{40}Ca in respect to a μ_1 signal for D1.

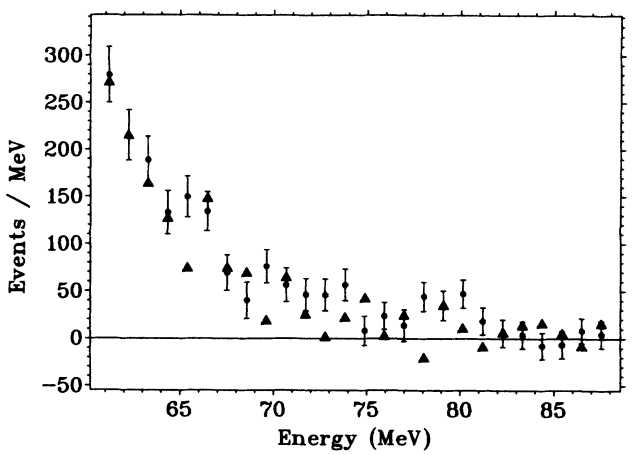

FIG. 11. Energy spectrum of events from the ^{209}Bi target which fired only one or two bars of the NaI wall [predominantly neutrons (open circles)] compared to the spectrum of events with more than two bars involved [predominantly photons (solid triangles)].

ed in Table I. The pion contamination was not homogeneous over the beam cross section. Therefore S_{pr} depended on the target because the muon and pion stop fractions in the degrader and in the targets respectively as well as the counting efficiencies were different for each hodoscope strip.

As Fig. 10 demonstrates, an appreciable part of the muon induced events falls into the prompt time region. Since the RPC energy spectra below 50 MeV nearly drop to zero,[27] this contribution can directly be obtained from the ratio (r_μ) of μ-decay events appearing in the prompt spectrum to the number of events in the pion-free spectra below 50 MeV. Thus, the number of oversubtracted muon events is

$$\frac{dN_\mu}{dE}=\frac{dN'_\mu}{dE}[1+(1+S_{pr})r_\mu] .$$

3. Subtraction of nontarget associated background

From our pion-free spectra we subtracted pion-free empty target runs with a subtraction factor S normalized to equal numbers of μ_1 counts. This removed every background caused by the beam. (As Fig. 2 shows, there is no material behind the target, i.e., "shadowing effects" may be excluded.) Since the muon intensity was not completely stable, a contribution from cosmic muons remained in the D2 spectra. We removed it by subtraction of data taken with the accelerator turned off, normalizing to the fraction f_4 of cosmic events above 200 MeV. Thus we obtained the signal from the target as

$$\frac{dN^{\text{target}}}{dE}=\frac{dN_\mu^{\text{in}}}{dE}-S\frac{dN_\mu^{\text{out}}}{dE}-f_4\frac{dN^{\text{cosmic}}}{dE} .$$

4. Analysis of neutron background

We determined the remaining neutron contribution in our spectra (including only events with more than two bars involved) by fitting spectra of the number of bars which fired for the full data set with a mixture of measured pure photon and pure neutron spectra [Fig. 7(b)]. This fit had to be carried out in energy bins of 10 MeV because the relevant distributions slowly vary with the photon energy. As Fig. 11 illustrates, the shape of the measured neutron spectra is very similar to the photon spectra. We, therefore, accounted for the neutron con-

TABLE I. Quantities involved in the pion event subtraction. The inefficiency of the prompt time cut is defined as $\bar{\epsilon}_\mu=S_{pr}/(1+S_{pr})$.

Target	Inefficiency of prompt cut $\bar{\epsilon}_{pr}$ D1	D2	Pion contribution in RMC energy region after prompt cut D1	D2	Muon contribution in prompt time window r_μ D1	D2
^{12}C		0.112±0.007		0.462±0.015		0.433±0.019
^{16}O		0.217±0.007		0.500±0.013		0.182±0.002
^{27}Al	0.161±0.011	0.257±0.008	0.130±0.006	0.282±0.008	0.261±0.003	0.205±0.003
^{40}Ca	0.153±0.010	0.231±0.007	0.082±0.004	0.164±0.005	0.158±0.003	0.173±0.003
^{nat}Fe	0.146±0.013	0.240±0.007	0.086±0.005	0.186±0.005	0.271±0.005	0.209±0.004
^{165}Ho	0.130±0.018	0.325±0.011	0.173±0.013	0.594±0.020	0.214±0.007	0.179±0.005
^{209}Bi	0.184±0.013	0.331±0.007	0.195±0.009	0.475±0.010	0.287±0.005	0.227±0.003
Empty	0.351±0.25	0.368±0.010	0.842±0.054	0.789±0.022	0.232±0.009	0.225±0.006

TABLE II. Background contributions in the RMC region (65 to 90 MeV).

Target	Empty target contribution D1	Empty target contribution D2	f_n (Neutrons) D2	f_{pu} (Pile-up) D1
^{12}C		0.522±0.098		
^{16}O		0.182±0.018	0.099±0.020	
^{27}Al	0.019±0.005	0.086±0.009	0.070±0.009	0.258
^{40}Ca	0.014±0.003	0.049±0.005	0.053±0.006	0.022
^{nat}Fe	0.020±0.005	0.060±0.006	0.049±0.006	0.025
^{165}Ho	0.080±0.019	0.345±0.034	0.116±0.048	0.009
^{209}Bi	0.064±0.016	0.201±0.021	0.185±0.019	0.015

tamination in photon spectra with an overall factor f_n (Table II).

5. *Correction for pile-up events*

We tested the possibility of event pile up in our detectors by comparing the spectral shapes of decay electrons at different beam intensities. While the NaI wall was completely insensitive to pile-up effects due to its modular structure, the big single crystal produced unphysical high energy events for light targets at maximum beam rate. A Monte Carlo program simulating the electronic arrangement and using the experimentally measured electron rates reproduced the measured distortion of the electron energy spectra exactly. We consequently calculated the probability for a bremsstrahlung photon to be pushed up into the RMC energy region by a part of an electron pulse falling into the 1 μsec ADC integration window of the two NaI crystals of D1. The calculated fractions f_{pu} of pile-up events in the RMC region are listed in Table II for the five heavier targets. For the lightest targets ^{12}C and ^{16}O the number of pile-up events was larger than twice the photon contribution. We therefore discarded all D1 data for these targets. This correction was only discovered after the preliminary analysis of our data from detector D1, presented in Ref. 35. This explains the too high capture rates for the two lightest targets given in the latter report.

B. Photon yield calculation

1. *Normalization*

In order to calculate the absolute photon yield a normalization factor N_0 was used for each spectrum

$$N_0=\frac{\mu_{st} f_{cap}(1-f_{abs})a_0}{(1-f_n)(1-f_{pu})} .$$

μ_{st} represents the number of muon stops in the target, f_{cap} is the percentage of the muons captured from the atomic orbit,[5] f_{abs} is the fraction of photons absorbed in the target, calculated for an average photon energy of 70 MeV,[28] and a_0 is the detector acceptance at 130 MeV. f_n and f_{pu} are the fractions of the remaining neutron and pile-up events, respectively.

2. *Fit procedure*

We made the fit to our data dN_μ/dE in the energy region between 65 and 95 MeV with the following expression:

$$\frac{dS}{dE}=N_0 B_\gamma(\Delta E)\int \frac{d\Lambda_N}{dE_\gamma} R(E,E_\gamma) r(E_\gamma) dE_\gamma .$$

$d\Lambda_N/dE_\gamma$ is the theoretical photon yield per captured muon normalized to 1 in the energy interval ΔE, i.e.,

$$\int_{\Delta E} \frac{d\Lambda_N}{dE_\gamma} dE_\gamma = 1$$

and $B_\gamma(\Delta E)$ is the total photon yield in ΔE (we chose the energy region above 57 MeV to be able to compare our results with those of other works.[6,7] $R(E,E_\gamma)$ represents the detector resolution function and $r(E_\gamma)$ the relative acceptance normalized to 1 at 130 MeV.

The free parameter was $B_\gamma(\Delta E)$ for the theories of "Chr81" and "CG85" and in addition the maximum photon energy k_{max} for the polynomial used by "CRS80." In

TABLE III. Fit intervals and event statistics.

Target	Detector D1 Fit interval (MeV)	Detector D1 Number of events	Detector D2 Fit interval (MeV)	Detector D2 Number of events
^{12}C			[71,88]	75±46
^{16}O	[65,92]	420±25	[65,90]	325±37
^{27}Al	[64,93]	613±29	[65,90]	889±46
^{40}Ca	[65,93]	946±36	[65,90]	2288±64
^{nat}Fe	[65,92]	609±29	[65,90]	1819±60
^{165}Ho	[64,85]	124±16	[65,85]	180±39
^{209}Bi	[66,91]	275±27	[65,85]	865±68

TABLE IV. RMC branching ratios per muon capture for photon energies ≥ 57 MeV; maximum photon energy k_{max} in closure approximation; χ^2 per degree of freedom.

		Detector D1			Detector D2		
Target	Applied theory	Branching ratio (10^{-5})	k_{max} (MeV)	χ^2	Branching ratio (10^{-5})	k_{max} (MeV)	χ^2
^{12}C	CG85				2.7 $\pm$1.8		0.89
^{16}O	CG85				2.44$\pm$0.47		0.93
	CRS80				2.39$\pm$0.46	89.9$\pm$5.0	0.91
^{27}Al	CRS80	$1.85^{+0.58}_{-0.25}$	86.8$\pm$1.8	0.75	$1.80^{+0.57}_{-0.25}$	90.8$\pm$1.8	1.25
^{40}Ca	Chr81	2.26$\pm$0.30		0.80	2.34$\pm$0.30		1.14
	CRS80	2.23$\pm$0.29	92.1$\pm$1.8	0.87	2.29$\pm$0.30	92.6$\pm$0.8	1.18
^{nat}Fe	CRS80	1.59$\pm$0.22	89.7$\pm$1.7	1.13	1.87$\pm$0.25	90.6$\pm$1.2	1.47
^{165}Ho	CRS80	0.91$\pm$0.18	83.7$\pm$5.3	0.70	0.58$\pm$0.19	85.1$\pm$11.4	0.78
^{209}Bi	CRS80	0.58$\pm$0.10	88.5$\pm$0.6	0.83	0.68$\pm$0.12	84.2$\pm$2.7	1.62

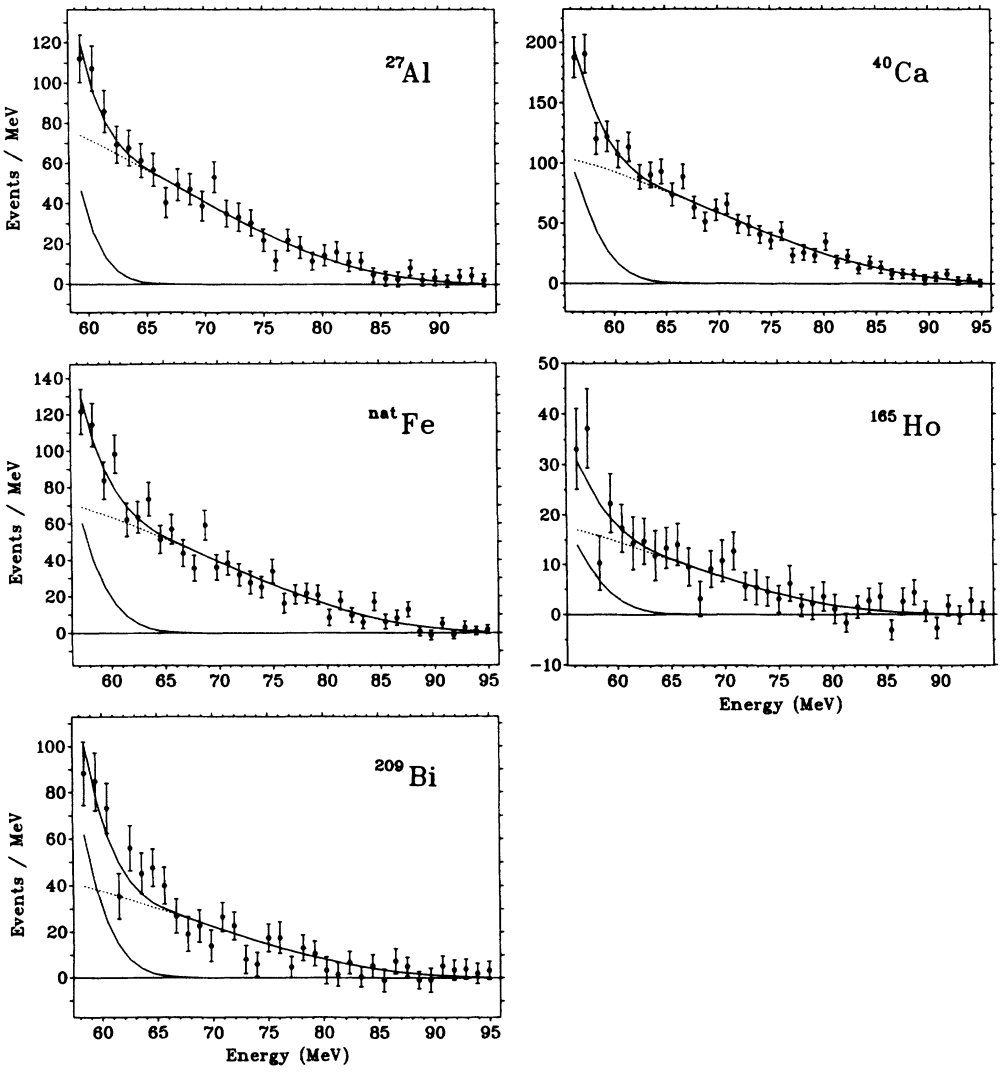

FIG. 12. Fitted RMC spectra for detector D1.

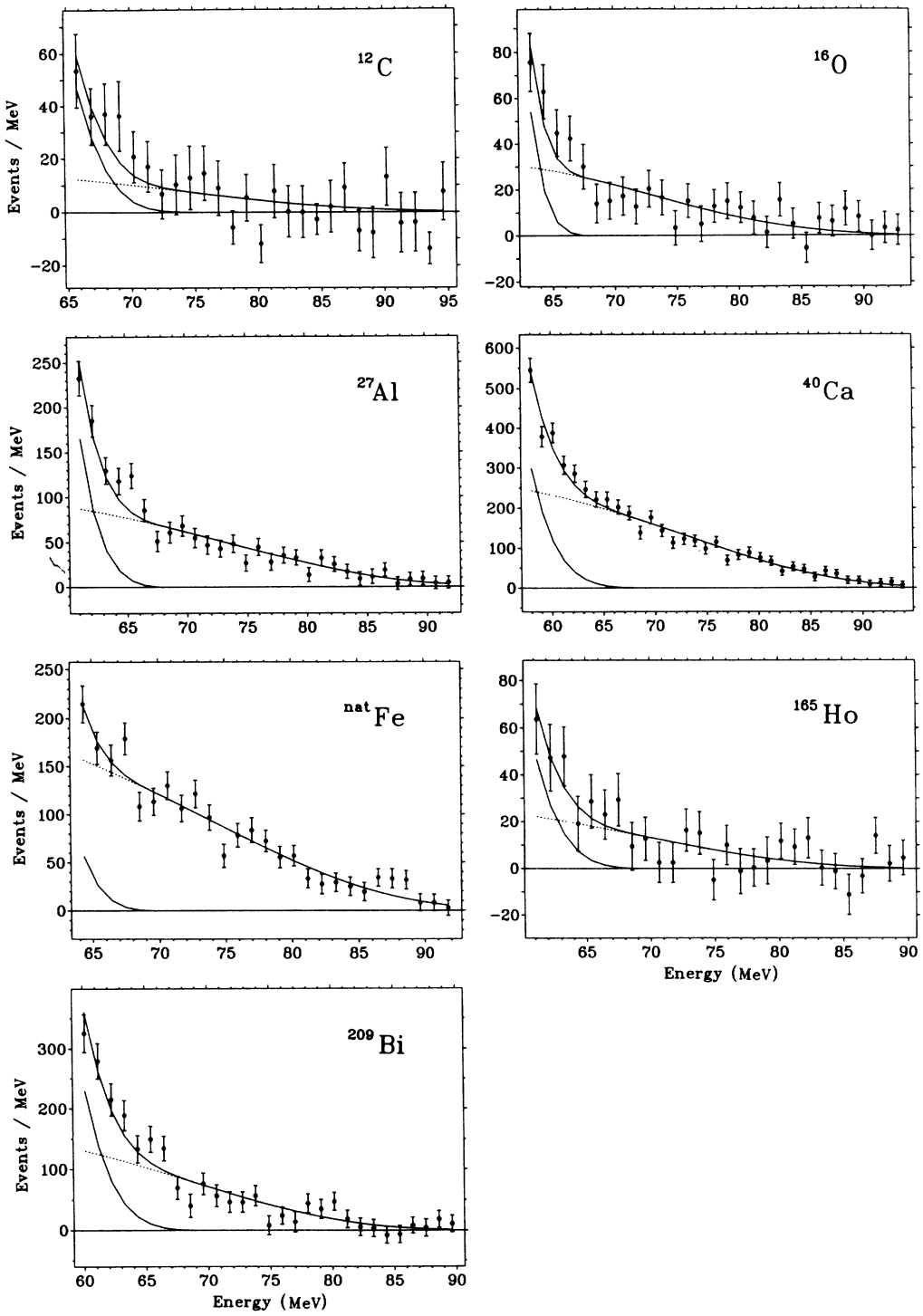

FIG. 13. Fitted RMC spectra for detector D2.

order to base the results on the experimental data we finally multiplied $B_\gamma(\Delta E)$ by the ratio of the actual number of events in the fitted energy region to the integral of the fitted curve in the same region.

V. RESULTS

Table III compiles the energy regions with the corresponding number of events that have been compared to the theoretical predictions. We fitted the polynomial spectrum of "CRS80" to all our data (except the ^{12}C data for which the statistics were not sufficient for a reasonable two parameter χ^2 fit). Table IV lists the values for the resulting RMC branching ratios B_γ above 57 MeV and the maximum photon energies k_{max}, while Figs. 12 and 13 show the fitted spectra. The calculation of "CRS80" has only been carried out for the nuclei $_{42}$Mo, $_{50}$Sn, $_{64}$Gd, $_{74}$W, $_{82}$Pb, $_{92}$U. In order to be able to extract

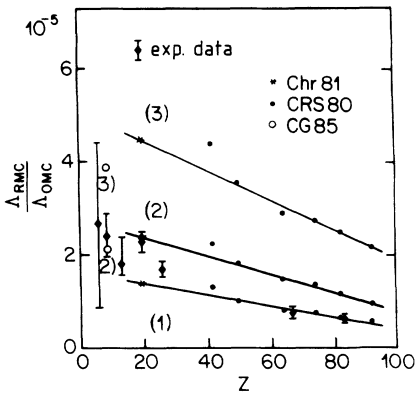

FIG. 14. Weighted means of the RMC branching ratios above 57 MeV for the two detectors compared to the theoretical predictions. (1) $g_P=0$, (2) $g_P=7g_A$, (3) $g_P=14g_A$.

a value for g_P from the measured RMC branching ratios of $^{27}_{13}$Al, $^{nat}_{26}$Fe, $^{nat}_{67}$Ho, and $^{209}_{83}$Bi, we extrapolated the theoretical branching ratios to all values of nuclear charge Z by a straight line starting from the ^{46}Ca branching ratio calculated by "Chr81" as illustrated in Fig. 14. The values obtained for g_P vs Z are shown in Fig. 15 and listed in Table V.

We determined the values of g_P for the ^{16}O and ^{40}Ca data with the specific models "CG85" and "Chr81." A comparison of the values for the χ^2 per degree of freedom to those obtained with the "CRS80" polynomial (Table IV) shows that the fit to the data was rather insensitive to the differences in the spectral shape used, a fact which has to be ascribed to the bad energy resolution.

For the ^{12}C data we adopted the "CG85" model.

A. Precision of the results

The errors given for B_γ and g_P (Tables IV and V) correspond to 1 standard deviation and include the statistical as well as the systematical errors.

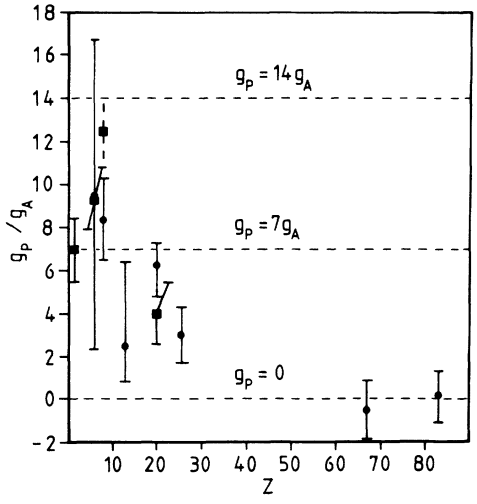

FIG. 15. Pseudoscalar coupling constant g_P vs nuclear charge Z. Solid circles: this experiment. Solid squares: see text.

TABLE V. Weighted means of the RMC branching ratios above 57 MeV for the two detectors and the resulting values for g_P following the indicated theories.

Target	Branching ratio (10^{-5})	g_P/g_A CRS80	CG85	Chr81
$^{12}_{6}$C	2.7 ±1.8	$7.2^{+5.6}_{-11.8}$	9.5±7.2	
$^{16}_{8}$O	2.44±0.47	$6.0^{+2.0}_{-3.0}$	8.4±1.9	
$^{27}_{13}$Al	$1.83^{+0.58}_{-0.25}$	$2.5^{+3.9}_{-1.7}$		
$^{40}_{20}$Ca	2.30±0.21	$6.3^{+1.0}_{-1.5}$		$6.3^{+1.0}_{-1.5}$
$^{nat}_{26}$Fe	1.71±0.17	3.0±1.3		
$^{165}_{67}$Ho	0.75±0.13	−0.5±1.4		
$^{209}_{83}$Bi	0.62±0.08	0.2±1.1		

The error of the number of events in the individual energy channels are correlated via the errors of the subtraction factors S_{pr}, S, f_4, and the common factor $[1+(1+S_{pr})r_\mu]$. The error of the total number of photon events in the considered energy region has therefore not been determined from the χ^2 fit but has been calculated by means of a Monte Carlo method varying the independent quantities within their normal distribution. The resulting values are, as expected, 20–30% higher than those given by the χ^2 fit. A fairly important contribution of 6–9% to the error of the number of photon events is due to the uncertainty of our energy calibration [0.8 MeV (D1), 0.7 MeV (D2)] at the low energy limit of the RMC region.

The uncertainty of the absolute normalization (N_0) includes contributions from the number of muon stops μ_{st} (7%), the captured fraction of muons f_{cap} (0.2–2.7%, see Table VI), and the absolute acceptance a_0 of the photon detectors [8% (D1), 9% (D2)]. The influence of the detector resolution on the branching ratios is small (<3% error). The errors of f_{abs} and f_{pu} have been neglected.

The extrapolated photon yield in the energy interval above 57 MeV depends on the theoretical spectral shape used below the experimental accessible energy region starting at 65 MeV. If, for example, the maximum photon energy k_{max} in the "CRS80" polynomial is changed from 90 to 91 MeV then the extrapolated photon yield between 57 and 65 MeV changes by 3% of the total yield above 57 MeV.

TABLE VI. Normalization factors.

Target	f_{cap}	f_{abs}
^{12}C	0.074 ±0.002	0.965
^{16}O	0.175 ±0.005	0.946
^{27}Al	0.606 ±0.002	0.941
^{40}Ca	0.844 ±0.002	0.919
^{nat}Fe	0.9064±0.0006	0.908
^{165}Ho	0.9659±0.0003	0.961
^{209}Bi	0.9666±0.0002	0.858

B. Comparison to previous data

Our data on ^{40}Ca are in good agreement with those of Refs. 6 and 7: $B_\gamma = (2.11 \pm 0.14) \times 10^{-5}$ and $B_\gamma = (2.07 \pm 0.20) \times 10^{-5}$, respectively. However, for ^{16}O we find a value which differs from the preliminary result of a pair spectrometer measurement quoted in Ref. 36; $B_\gamma = (6.2 \pm 0.8) \times 10^{-5}$ by four combined standard deviations. Figure 16 shows a comparison of the "unfolded" spectra, i.e., the spectra have been shifted by the average displacement of the resolution function from the true energy and the normalization factors have been divided out. This technique was proven to give identical results to the comparison with correctly folded theoretical curves in the narrow resolution pairspectrometer case, in the low resolution data reported here it serves mainly to indicate the possible origin of the discrepancy. The difference seems to arise mainly from the overall normalization (and/or background subtraction), not from the extrapolation (down to 57 MeV) using theoretical predictions, since already the high energy data above 65 MeV differ by nearly a factor of 2. For a more complete discussion one must await the final analysis of the pair spectrometer data.

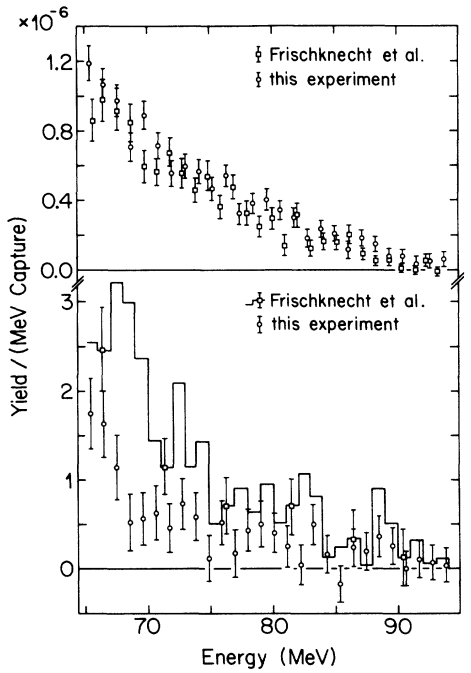

FIG. 16. Comparison of the photon spectra for ^{16}O (bottom) and ^{40}Ca (top) with previous data. Open circles: this experiment. Top: solid squares, Ref. 7. Bottom: histogram, Ref. 36.

VI. CONCLUSIONS

The data obtained in this experiment allow a first view of the behavior of the induced pseudoscalar coupling in nuclei, if further more refined theoretical calculations should back up the expectations based on the Fermi gas model. Within the limited precision, dictated by background conditions adverse to measuring the rare radiative muon capture process, the relative importance of the radiative branch seems to decrease with increasing nuclear mass indicating a nearly complete quenching for heavy systems. Such a behavior has been predicted by Delorme *et al.*[13] In the nuclear matter limit g_A approaches 1 and g_P approaches 0, as for a bare Dirac particle. For finite systems g_P decreases with the nuclear size to about 30% of the nucleonic value for large nuclei ($R > 4$ fm) in this calculation. However, the authors themselves caution the direct application of their predictions to radiative muon capture, because their treatment applies mainly to the spatial part of the pseudoscalar current, not to the time part, which is measured in our experiment. However, the dramatic renormalization effects, which appear in the comparison to the model calculations certainly warrant a fresh look at these predictions and hopefully also stimulate an extended experimental program.

In view of the good agreement for ^{40}Ca among various measurements, additional experimental data for ^{16}O and heavier nuclei are desirable.

ACKNOWLEDGMENTS

We thank Dr. M. Gmitro for valuable discussions on radiative muon capture calculations. The experiment was strongly supported by Prof. J. P. Blaser and his SIN crew. Further support was received from the Swiss funding agency for basic research, Schweizerischer Nationalfonds.

*Present address: Clinique de l'Université, Bruxelles, Belgium.
†Present address: Stanford Linear Accelerator Center, Stanford, CA 94305.
‡Present address: Lawrence Berkeley Laboratory, University of California, Berkeley, CA 94720.
§Present address: National Laboratory for High Energy Physics, Ibaraki-ken 305, Japan.

[1]L. Wolfenstein, in *High Energy Physics and Nuclear Structure,* edited by S. Devons (Plenum, New York, 1970), p. 661.
[2]G. Bardin *et al.*, Nucl. Phys. **A352**, 365 (1981).
[3]L. Ph. Roesch, V. L. Telegdi, P. Truttmann, A. Zehnder, L. Grenacs, and L. Palffy, Helv. Phys. Acta **55**, 74 (1982).
[4]A. R. Heath and G. T. Garvey, Phys. Rev. C **31**, 2190 (1985).
[5]M. Eckhause, R. T. Siegel, and R. E. Welsh, Nucl. Phys. **81**, 575 (1966); see also T. Suzuki, D. F. Measday, and J. P. Roalsvig, Phys. Rev. C **35**, 2212 (1987).
[6]R. D. Hart *et al.*, Phys. Rev. Lett. **39**, 399 (1977).
[7]A. Frischknecht *et al.*, Phys. Rev. C **32**, 1506 (1985).
[8]P. Christillin, Nucl. Phys. **A362**, 391 (1981).
[9]M. Gmitro, A. Ovchinnikova, and T. V. Tetereva, Nucl. Phys. **A453**, 685 (1986).
[10]For detailed references on these three phenomena see, e.g., *Weak and Electromagnetic Interaction in Nuclei,* edited by H. V. Klapdor (Springer-Verlag, Berlin, 1986), p. 260.
[11]M. Ericson, Prog. Part. Nucl. Phys. **1**, 67 (1978).
[12]M. Ericson, in *Mesons in Nuclei,* edited by M. Rho and D.

Wilkinson (North-Holland, Amsterdam, 1979), Vol. III, p. 905.
[13]J. Delorme, M. Ericson, A. Figureau, and C. Thévenet, Ann. Phys. (N.Y.) **102**, 273 (1976).
[14]M. Gmitro and P. Truöl, Adv. Nucl. Phys. **18** (1987).
[15]H. P. C. Rood and H. A. Tolhoek, Nucl. Phys. **70**, 658 (1965).
[16]P. Christillin and S. Servadio, Nuovo Cimento **42**, 165 (1977).
[17]M. Gmitro and A. Ovchinnikova, Nucl. Phys. **A356**, 323 (1981).
[18]M. Ericson, A. Figureau, and C. Thévenet, Phys. Lett. **45B**, 19 (1973).
[19]K. Ohta, Phys. Rev. Lett. **33**, 1507 (1974).
[20]E. C. Akhmedov, T. V. Tetereva, and R. A. Eramzhyan, Sov. J. Nucl. Phys. **42**, 67 (1986).
[21]L. L. Foldy and J. D. Walecka, Nuovo Cimento **34**, 1026 (1964).
[22]P. Christillin and M. Gmitro, Phys. Lett. **150B**, 50 (1985).
[23]P. Christillin, M. Rosa-Clot, and S. Servadio, Nucl. Phys. **A345**, 331 (1980).
[24]A. Bay, Ph.D. thesis, Université de Lausanne, 1986; A. Bay *et al.*, Phys. Lett. B **174**, 445 (1986); see also, A. Bay *et al.*, Nucl. Instrum. Methods (in press).
[25]M. Döbeli, Ph.D. thesis, Universität Zürich, 1987.
[26]R. L. Ford and W. R. Nelson, SLAC Report 210, UC-32, 1978.
[27]M. Gmitro, P. Truöl, H. Kissener, and R. A. Eramzhyan, Sov. J. Part. Nucl. **14**, 323 (1983).
[28]J. H. Hubbel *et al.*, J. Phys. Chem. Ref. Data **9**, 1043 (1980).
[29]N. Morel, Ph.D. thesis, Université de Lausanne, 1979; see also, J. C. Alder *et al.*, Nucl. Instrum. Methods **160**, 93 (1979). The average of older measurements (1962–1971) gives 1.37 ± 0.07; see, e.g., J. Bistirlich *et al.*, Phys. Rev. C **5**, 1867 (1972).
[30]J. Spuller *et al.*, Phys. Lett. **67B**, 479 (1977).
[31]T. Kozlowski *et al.*, Nucl. Phys. **A436**, 717 (1985).
[32]A. Bol *et al.*, Nucl. Instrum. Methods **202**, 511 (1982).
[33]J. A. Lezniak, Nucl. Instrum. Methods **136**, 299 (1976).
[34]P. Hänggi *et al.*, Phys. Lett. **51B**, 119 (1974).
[35]M. Döbeli *et al.*, in *Weak and Electromagnetic Interaction in Nuclei,* edited by H. V. Klapdor (Springer-Verlag, Berlin, 1986), p. 822.
[36]A. Frischknecht *et al.*, Czech. J. Phys. **B32**, 270 (1982).